







Atomic mechanism of the phase transition in monolayer bismuthene on copper oxide

Dechun Zhou ^{1,*}, Chao Yang,^{2,*} Saiyu Bu ^{3,*},†, Feng Pan ⁴, Nan Si,¹ Pimo He,² Qingmin Ji ¹, Yunhao Lu ^{2,‡} and Tianchao Niu ^{1,§}¹Herbert Gleiter Institute of Nanoscience, School of Material Science and Engineering, Nanjing University of Science & Technology, Nanjing 210094, China²Department of Physics, Zhejiang University, Hangzhou 310027, China³School of Mechanical Engineering, Shanghai Jiao Tong University, Shanghai 200240, China⁴Research Institute for Frontier Science of Beihang University, Beihang University, Beijing, 100083, China

(Received 24 November 2020; revised 30 March 2021; accepted 14 May 2021; published 3 June 2021)

Problems associated with large-scale growth of high-quality single-layer bismuthene constitute one of the main obstacles to the applications of bismuthene in electronic devices. Here we report the direct synthesis of high-quality bismuthene using molecular-beam epitaxy on dielectric copper oxide thin films. Scanning tunneling microscopy (STM) reveals the generation of dimer pair arrays and black-phosphorus-like bismuthene (BKP-Bi, α phase) at the initial stage on $\text{Cu}_3\text{O}_2/\text{Cu}(111)$ surface. A phase transition from BKP-Bi to blue-phosphorus-like bismuthene (BLP-Bi, β phase) is characterized by high-resolution STM, complemented with first-principles calculations based on density-functional theory (DFT) showing a bond-breaking path. Employing the phase transition, we also demonstrate the construction of an atomically sharp in-plane homojunction along the phase boundary. DFT calculations reveal a one-dimensional edge state along the homojunction.

DOI: [10.1103/PhysRevMaterials.5.064002](https://doi.org/10.1103/PhysRevMaterials.5.064002)

I. INTRODUCTION

Bismuth (Bi, $Z = 83$), the heaviest nonradioactive element, has attracted a tremendous amount of attention from the materials and physics community owing to its strong spin-orbit coupling (SOC) that makes it a promising candidate for topological systems [1–5]. In particular, freestanding single layer of blue-phosphorus-like (BLP, β phase) Bi(111), bismuthene, is regarded as a two-dimensional (2D) topological insulator (TI) with the largest nontrivial gap (0.6 eV) [6–9]. In addition, its 2D allotrope adopting black-phosphorus-like (BKP, α phase) puckered structure exhibits topological properties when the Bi atoms in the top layer have a buckling height less than 0.1 Å [10,11].

Abundant efforts have been devoted to the synthesis of these 2D allotropes on a variety of substrates that the substrate registry and/or orbital-filtering effect contributes to the stabilization of the wide-gap quantum spin Hall phase [12,13]. However, preparation of bismuthene film with well-controlled properties is still a daunting challenge that requires a comprehensive understanding of the growth mechanism at the atomic scale [14]. In previous investigations, Bi started from a three-monolayer base featuring an α phase on weakly interacted graphite surface at room temperature [15]. However, single-layer α -bismuthene can be stabilized on graphite at low substrate temperature (~ 220 K), while the second layer

exhibits a β phase [16]. On metallic surfaces, such as Ni [17,18], Cu [19,20], and Ag [21,22], Bi tends to form surface alloy at initial stage. Dealloying occurs after increase in coverage that finally results in β phase. On a chemically inert substrate, Au(111), Bi aggregates into $p \times \sqrt{3}$ stripe arrays at the first atomic layer, and transits to α phase from the second to 60 layers [23–27]. On semiconducting Si(111) [28–31] and Ge(111) [32–34] surfaces, Bi also shows a phase transition as a function of layer thickness that α phase is stabilized at low coverage and transforms into β phase above six layers. To circumvent the difficulties in preparing a single-layer bismuthene, one effective approach is to deposit directly on Bi-based TIs, such as Bi_2Te_3 [35–37], Bi_2Se_3 , and $\text{Bi}_2\text{Te}_2\text{Se}$ [38], on which β phase is favorable. On 1T-TaSe₂ [39] and NbSe₂ [40–43], which belong to charge-density wave and superconducting compounds, α phase can be stabilized.

As demonstrated above, substrate and temperature are key factors in determining the as-prepared phases that have been applied to the phase engineering of other group 15 elemental Xenes [44]. For example, theoretically, freestanding BKP is more stable than BLP regardless of the temperature. There is an energy barrier of 0.48 eV/atom when BKP transforms to BLP that is kinetically unlikely. However, when placing on Au(111), BLP is more stable than BKP, suggesting that the substrate strongly influences the phase diagram [45]. The substrate-governed phase engineering has also been experimentally and theoretically explored in the phase transition of antimonene [46,47]. On Bi_2Se_3 , α -antimonene dominated at room temperature, but transformed to β phase after annealing at 473K via an asymmetric bond-breaking path because of the specific lattice matching between the β -antimonene and Bi_2Se_3 . Nonetheless, on twofold symmetric substrates, such

*These authors contributed equally to this work

†busaiyu@sjtu.edu.cn

‡luyh@zju.edu.cn

§tcniu@njust.edu.cn

as WTe_2 [48] and SnSe [47], antimonene adopted the puckered honeycomb lattice (α phase) due to as well the lattice registry. Therefore, understanding the growth mechanism is of paramount importance to delicately tune the phases of these elemental Xenes, which is vital for their applications in topological systems [49,50].

Here, we successfully grow single-layer α - and β -bismuthene on $\text{Cu}_3\text{O}_2/\text{Cu}(111)$ by using molecular-beam epitaxy (MBE). We present the phase transition from α - to β -bismuthene induced by thermal annealing. Properties of both phases and the phase transition processes are revealed by high-resolution scanning tunneling microscopy (STM) at the atomic scale. DFT-based first-principles calculations comprehensively explain a bond-breaking pathway. Finally, an in-plane homojunction with sharp atomic interface is constructed at the phase boundary between α - and β -bismuthene, which demonstrates one-dimensional edge state.

II. EXPERIMENTS

A. Sample preparation and STM measurements

Sample preparation and STM measurements were performed in a SPECS Joule-Thomson scanning probe microscopy system comprising of an ultrahigh-vacuum MBE chamber and a probe chamber with a base pressure better than 2×10^{-10} mbar [51]. All the samples were prepared in the MBE chamber, and transferred directly to the STM chamber without breaking the vacuum. Single crystals of $\text{Cu}(111)$ were cleaned by repeated Ar^+ sputtering (1 kV, 10^{-5} mbar, 15 min) and annealing cycles (700 K, 10 min). Bi was deposited from a thermal evaporator onto the substrate held at 370 K. All the STM images were taken at 77 K with a tungsten tip, and the bias voltages were defined as the sample bias.

B. Computational techniques

The first-principles calculations are based on DFT, as implemented in the Vienna *Ab initio* Simulation Package [52]. The Perdew-Burke-Ernzerhof [53] realization of the generalized gradient approximation was used for the exchange correlation. The projector augmented wave [54] method was employed to model the ionic potentials. The energy cutoff was set to 500 eV for all calculations. A vacuum space of 20 Å was introduced to avoid interactions between structures. In all geometry optimizations, van der Waals (vdW) correction (in Grimme-D2 approach) was considered [55]. All the atoms are allowed to relax until the calculated forces are less than 0.01 eV/Å, while the electronic minimization was applied with a tolerance of 10^{-6} eV. The Monkhorst-Pack k -point sampling was used for the Brillouin-zone integration: $10 \times 12 \times 1$ for α -bismuthene, $12 \times 12 \times 1$ for β -bismuthene which unit cell is rhomboid, $8 \times 12 \times 1$ for $\text{Bi}(111)$ which unit cell is rectangular, $1 \times 12 \times 1$ for the α - β homojunction, $3 \times 5 \times 1$ for the α -bismuthene on the $\text{Cu}_3\text{O}_2/\text{Cu}(111)$, and $1 \times 1 \times 1$ for the β -bismuthene on the $\text{Cu}_3\text{O}_2/\text{Cu}(111)$. The phase transition in freestanding bismuthene was simulated using the variable-cell nudged elastic band scheme (VC-NEB) [46,56], as implemented in the USPEX code [57,58]. Within the two pathways, both the α - and β -bismuthene are allowed to relax freely, while the lattice constants of transition state 1

(TS1) are fixed during optimization. Furthermore, the x - and y coordinates are also fixed for other structures.

III. RESULTS AND DISCUSSION

A. Coverage- and temperature-dependent phase transition

To prohibit the formation of substitutional surface alloy [19], a buffer layer is introduced by simply annealing $\text{Cu}(111)$ single crystal at 650 K in oxygen to generate an oxide thin film [59] (Fig. S1 in the Supplemental Material [60]). Figure 1(a) shows an STM image of the oxide surface after Bi deposition at 370 K in the submonolayer regime. Bi atoms assemble into dimer arrays with a square unit cell of $1.35 \text{ nm} \times 1.35 \text{ nm}$ [inset in Fig. 1(a)]. Increasing the coverage to 1 ML, Bi adatoms pack densely to form short-range ordered atomic islands with an average interatomic distance of 0.4 nm that span over the entire surface [Fig. 1(b)]. Annealing for 10 min at 470 K generates domains possessing different orientations together with isolated clusters [circles in Fig. 1(c)]. An angle of 60° in neighboring domains indicates a threefold symmetric substrate underneath. The zigzag structure with a rectangle unit cell of $0.46 \text{ nm} \times 0.51 \text{ nm}$ suggests the formation of α -bismuthene [61]. Such growth mode differs greatly from that on clean $\text{Cu}(111)$ homogeneous reparation of Bi atoms occurs to form substitutional $\text{BiCu}_2(111)$ surface alloy [19]. In Fig. 1(d), we show two terraces consisting of α - and β -bismuthene, respectively, which illustrates evolution of β phase after annealing at 500 K for 20 min. Zoom-in scans are taken across bright strips showing the mirror twin boundaries and atomic lattices of the α - and β -bismuthene, respectively [insets in Fig. 1(d)]. A mirror twin boundary consists of distorted lattice in both sides linked by Bi atoms propagating along the dislocation lines [62]. The measured unit-cell sizes of α - and β -bismuthene are $0.45 \text{ nm} \times 0.52 \text{ nm}$, and $0.45 \text{ nm} \times 0.45 \text{ nm}$, respectively, close to the values of freestanding single-layer cases (measured line profiles in Fig. S2 within the Supplemental Material [60]) [11,43]. After more than 40 min annealing, the surface is covered by uniform β -bismuthene [Fig. 1(e)]. The atomically resolved STM image [inset in Fig. 1(e)] reveals distinctly the hexagonal structure that matches well with the atomic termination of β -bismuthene. The fast Fourier transform (FFT) shows the hexagonal lattice on the measured terraces [inset in Fig. 1(e)]. Figure 1(f) is the time rate of change of surface ratio, going from a β -phase free surface to being completely covered with β -bismuthene. More STM images can be found in Fig. S3 in the Supplemental Material [60]. Furthermore, we also performed high-temperature annealing that showed 530 K for 10 min is sufficient to complete the phase transition. This feature verifies that the ripening of β phase is qualitatively proportional to the annealing temperature [46].

B. Phase transition mechanisms

Figures 2(a) and 2(b) demonstrate the optimized configurations of freestanding α - and β -bismuthene, respectively (for DFT details see Computational techniques in Section II: Experiments). Examining their atomic structures, one can see that the unit-cell size (4.42 Å) along the x axis of α -bismuthene is coincident with that along the zigzag edge of

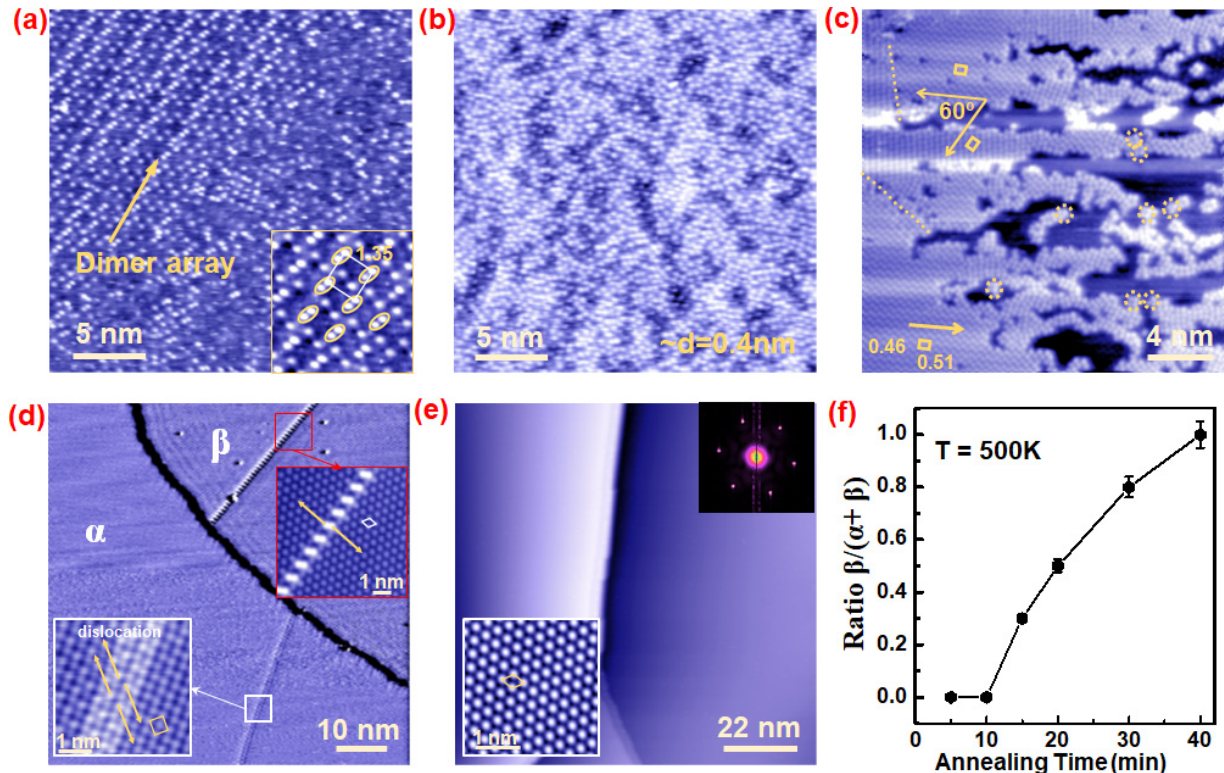


FIG. 1. Coverage- and temperature-dependent structural evolution of Bi atomic layer on $\text{Cu}_3\text{O}_2/\text{Cu}(111)$. (a) 0.5 monolayer (ML) [1 ML equals a fully covered Bi(111) layer] Bi deposited on the substrate held at 370 K; inset is a high-resolution STM image of the Bi dimer array. (b) Increasing the coverage to 1 ML without annealing. (c) Annealing at 470 K for 10 min. (d) Subsequent annealing at 500 K for 20 min; insets are high-resolution STM images of the α - and β -bismuthene, respectively. (e) 500 K annealing for 40 min; insets present the FFT pattern and atomic lattice of the β -bismuthene. (f) Ratio of β -bismuthene to both phases as a function of annealing time. The annealing temperature is 500 K. Scanning parameters: (a) 2.5 V, 90 pA; (b) 1.5 V, 67 pA; (c) 2.5 V, 80 pA; (d) 1.2 V, 90 pA; (e) 0.6 V, 100 pA.

β -bismuthene. This coincidence masks an atomically sharp in-plane epitaxy along the phase boundary. Meanwhile, formation of such an interface involves the phase transition process that needs to conquer a barrier [46]. Figure 2(c) shows two kinds of boundaries displaying distinctly different atomic structures with a rotation angle of 120° . Enlarged STM image of Fig. 2(d) (type I) shows an atomically sharp interface. The line profile (right panel) taken perpendicular to the boundary and across the y axis of both phases illustrates the formation of a homojunction, as shown below. The measured line profile demonstrates a height difference in a range of 0.17 to 0.50 Å (α - β) that depends strongly on the sample bias (see Fig. S4 in the Supplemental Material [60] for more STM images). These values are much lower than the typical thickness of a single-layer bismuthene [16]. Meanwhile, it is also interesting to note that the β phase is higher than α phase in the bias range from -1.2 to $+1.5$ V. This feature is in striking contrast to theoretically optimized layer thickness that the puckered α phase is 1.6 Å higher than the buckled β phase. Since STM image contains both topographical and electronic density information, the unusual height difference between such an in-plane homojunction should be correlated to the different local density of state (DOS). STM image [Fig. 2(e)] distinctly reveals disordered Bi atoms in the α -bismuthene lattice (edge II), which rotate by 120° with respect to the sharp edge I. This feature is reasonable because 120° rotation generates no ordered atomic structure of α -bismuthene to bond with the

zigzag edge of β phase [atomic models in Figs. 2(a) and 2(b)], implying a possible bond-breaking pathway.

To get deep insight into the mechanism of phase transition, we adopted the VC-NEB scheme to model the transition processes from α - to β -bismuthene. Similar approaches have been applied to simulate the α to β -phase transition of phosphorene [63] and antimonene [46]. Firstly, we consider a similar approach with the conversion from puckered BKP to buckled BLP by introducing an array of dislocation [63], as depicted schematically in Fig. 3(a). Briefly, the transition process involves the stretching of α -bismuthene along the y axis, followed by the out-of-plane displacement of atoms in the reaction coordinates 2–8 [Fig. 3(b)]. The relative energy of structure 8 (β -bismuthene) is higher than that of structure 1, so it is distinct that α phase is more stable than β phase.

The second approach is a bond flipping path. As shown in their atomic structures, both α - and β -bismuthene consist of a honeycomb subunit adopting puckered and buckled structure, respectively. Thus, the direct transition from puckered structure to buckled configuration through flipping the bonds connecting the hexagons is reasonable. As depicted in Fig. 3(c), the lattice expands along the y axis (TS1) to offer enough space for the bond flipping. TS1 comprises flat sp^2 -like geometry of Bi atoms in the flipping process that requires an energy barrier of 0.31 eV/atom. This energy is comparable to that of the predicted transition via introducing an array of dislocation [Fig. 3(b)]. TS2 also experiences sp^2 -like geome-

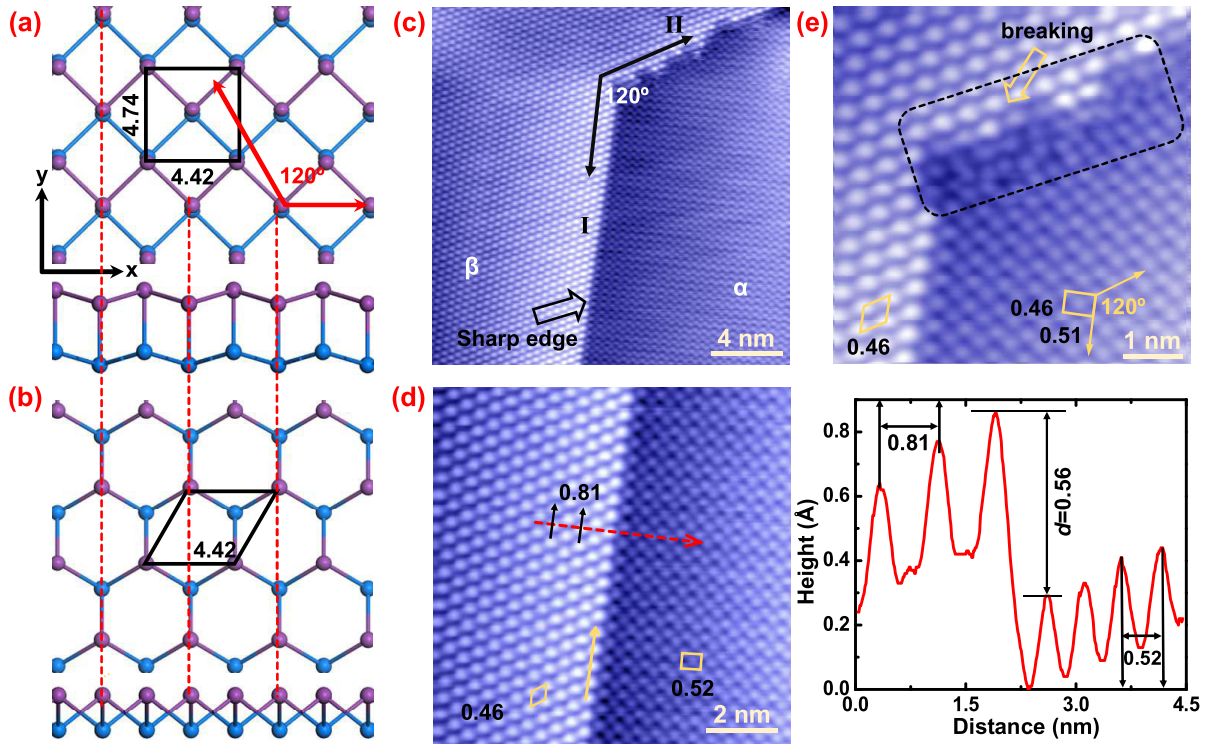


FIG. 2. Domain boundaries between α - and β -bismuthene. Atomic model of freestanding (a) α -bismuthene with a buckling height of 0.65 Å and (b) β -bismuthene. Top panels: top view. Bottom panels: side view. The unit cells are marked by black lines. The dashed red lines show the matched lattice constant between α - and β -bismuthene along the x axis. Purple and blue balls represent the upper and lower Bi atoms, respectively. (c) Two different boundaries (I and II) between α - and β -bismuthene on the $\text{Cu}_3\text{O}_2/\text{Cu}(111)$ surface. (d) Enlarged STM image of edge I with sharp interface and measured line profile along the red arrow. (e) Edge II with broken bonds. Scanning parameters: (c)–(e) 1.2 V, 90 pA.

try and bond flipping. The energy increases by 0.06 eV/atom from TS1 to TS2, while it decreases by 0.318 eV/atom to the final β -bismuthene.

Another transition pathway involving bond breaking is calculated which exhibits a lower energy barrier but more complicated than other cases. As plotted in Fig. 3(d), at the

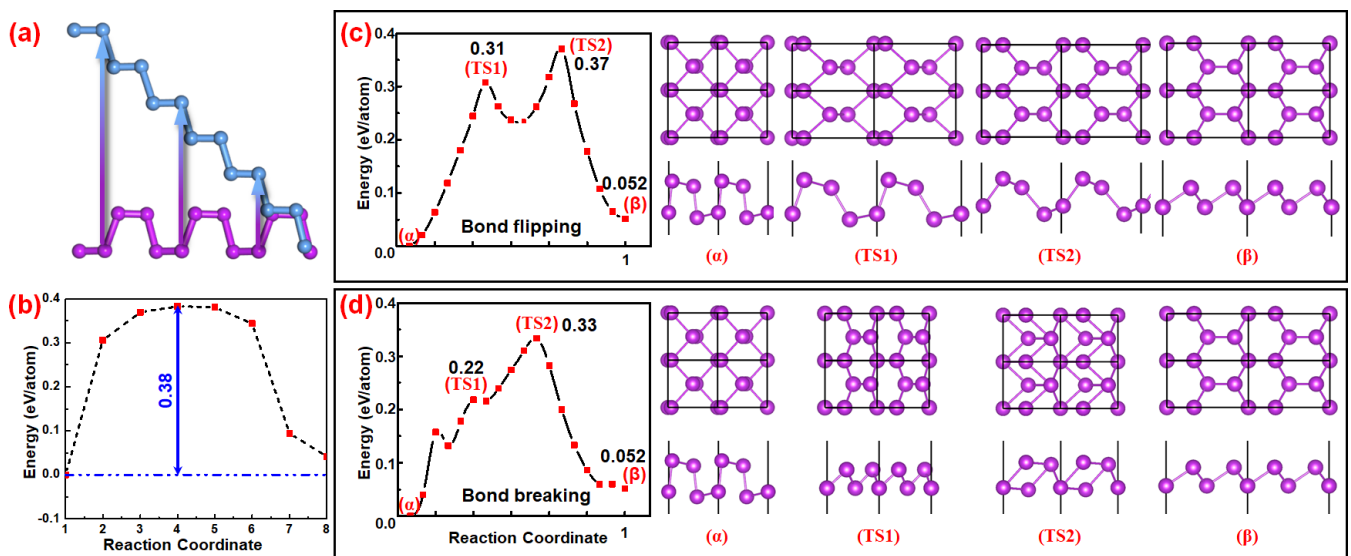


FIG. 3. Different transition pathways from α - to β -bismuthene. (a) Schematic of the transition by introducing dislocations, highlighted by the arrows. (b) Total energy change during the phase transition via introducing dislocations. (c) Energy change during bonding flipping path. Transition state 1 (TS1) and transition state 2 (TS2) present the extension of unit cell with elongated bond lengths. (d) Bond-breaking path. It involves the lattice distortion (TS1) and bond breaking (TS2).

initial stage, the unit cell remains fairly constant (TS1) where only considerable distortion occurs with a low-energy barrier of 0.22 eV/atom. Bond breaking occurs from TS1 to TS2 path where TS2 displays linear zigzag chains adopting buckled structure. This process differs from antimonene, where the bonding breaking occurs at TS1 that undergoes a local minimum state before reaching TS2. Lattice expansion takes place in the next stage to form preliminary structure of the β phase. The energy barrier is identified at 0.33 eV/atom. Our calculated barrier is higher than the reported $\alpha \rightarrow \beta$ transition of antimonene [46] via the similar path of bond breaking, but lower than that of phosphorene [63], even though the bond dissociation energy of Bi-Bi is the lowest [64].

C. Electronic structures of homojunction

Large-scale STM images demonstrate single-crystalline growth of β -bismuthene on each terrace. Furthermore, there is no isolated domain of β phase surrounded by α phase, indicating that the phase transition develops from step edges. In contrast to P and Sb, where sequential deposition and annealing on copper oxide leads to only the buckled-honeycomb β phase [59,65], Bi on $\text{Cu}_3\text{O}_2/\text{Cu}(111)$ generates single-layer puckered α phase at the initial stage. Consequently, a comprehensive understanding of the in-plane homojunction with sharp atomic interface comprising TIs can be reached. Single-layer β -bismuthene is a nontrivial TI, while α -bismuthene with a buckling height less than 0.1 Å has been proved to be a TI as well [11].

To illustrate their electronic properties, we performed DFT calculations. We considered two kinds of α -bismuthene with different buckling heights and the β -bismuthene, respectively. Their band structures considering the SOC are shown in Fig. S5 in the Supplemental Material [60]. Our results reproduce well with previous studies [11]. The buckled α -bismuthene (buckling height = 0.65 Å) Figures S5(a)–S5(c) show the normal band structure with an indirect band gap of 0.11 eV (SOC). Both the flat α -bismuthene ($h = 0$) and the β -bismuthene are nontrivial TIs with a band gap of 0.08 and 0.37 eV, respectively [Figs. S5(d)–S5(I)]. Placing bismuthene on $\text{Cu}_3\text{O}_2/\text{Cu}(111)$ substrate, we further investigated the interaction between α - and β -bismuthene and the substrate, respectively, as shown in Fig. 4. The lattice constants of bismuthene are optimized based on the measured STM data that suggest tensile strain for both cases. Comparing with their freestanding counterparts, the lattice variation upon placing on the substrate affects only the band-gap size, but has no impact on their topological properties (Fig. S6 in the Supplemental Material [60]). The α -bismuthene with a buckling height of 0.65 Å is a trivial semiconductor with an indirect band gap of 0.14 eV [0.20 eV with SOC, Figs. S6(a)–S6(c)]. However, the flat α -bismuthene shows a nontrivial band gap of 0.15 eV [0.14 eV with SOC, Figs. S6(d)–S6(f)]. The β -bismuthene also shows a nontrivial band gap but with a larger value of 0.54 eV [0.24 eV with SOC, Figs. S6(g)–S6(i)]. On $\text{Cu}_3\text{O}_2/\text{Cu}(111)$ surface, α -bismuthene adopts the puckered structure with a buckling height of 0.65 Å and an interlayer distance of 2.21 Å [Fig. 4(a)]. It is worth noting that the optimized α -bismuthene shows a buckling height even when using a flat α -bismuthene

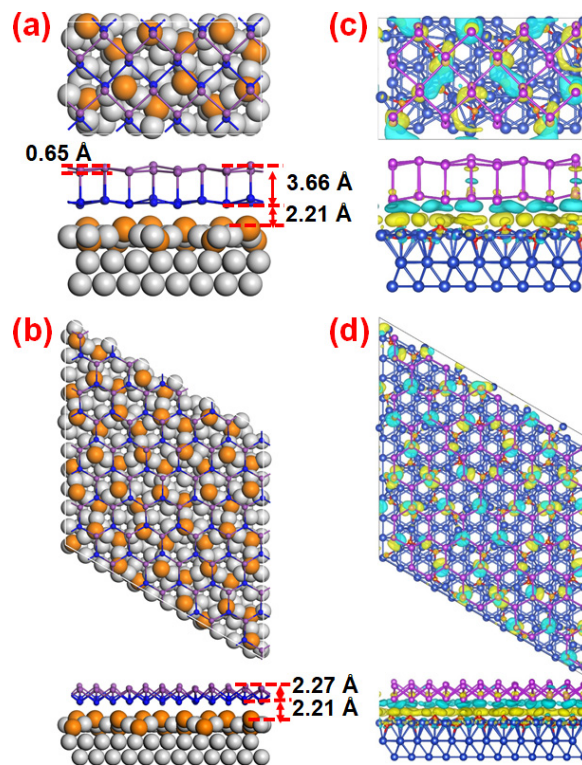


FIG. 4. DFT calculated atomic structures and interfacial properties of α - and β -bismuthene on the $\text{Cu}_3\text{O}_2/\text{Cu}(111)$ substrate. Top and side views of (a) α - and (b) β -bismuthene on $\text{Cu}_3\text{O}_2/\text{Cu}(111)$ substrate. Gray, orange, purple, and blue balls represent the copper, oxygen, upper Bi, and lower Bi atoms, respectively. The charge-density difference of (c) α - and (d) β -bismuthene on $\text{Cu}_3\text{O}_2/\text{Cu}(111)$ substrate. Yellow and blue colors represent the gain and loss of electrons, respectively.

as the initial structure. Regarding the β -bismuthene, the layer thickness increases to 2.27 Å on $\text{Cu}_3\text{O}_2/\text{Cu}(111)$ surface comparing to freestanding monolayer (1.67 Å). The distance between the Bi atoms in the bottom layer and the substrate is 2.21 Å, suggesting a weak vdW interaction. The binding energy of β -bismuthene on $\text{Cu}_3\text{O}_2/\text{Cu}(111)$ is 55 meV/Bi atom, which is 4 meV/Bi atom larger than the α phase. Therefore, the β -bismuthene is more energetically favorable when being placed on a substrate. Nonetheless, there is still remarkable electron transfer from the lower Bi atoms to the $\text{Cu}_3\text{O}_2/\text{Cu}(111)$ substrate for both cases, as shown in the charge-density plots [Figs. 4(c) and 4(d)].

To further reveal the electronic properties of the in-plane homojunction with a sharp atomic interface, we focus on the phase boundary between the α - and β -bismuthene. Due to the limitation of computational efficiency, we studied an ~ 10 -nm periodic cell with freestanding α - and β -bismuthene without considering the $\text{Cu}_3\text{O}_2/\text{Cu}(111)$ substrate (Fig. S7(a) in the Supplemental Material [60]). Remarkably, STM image shows an ordered zigzag edge in the β -bismuthene side [Fig. 5(a)]. The self-consistent calculations show that the zigzag termination points upward and is bonded with the top Bi atoms in α -bismuthene [Fig. 5(b)]. The simulated STM image reproduces well the experimental result [Fig. 5(c)] that the atoms along the boundary are brighter than surroundings. The

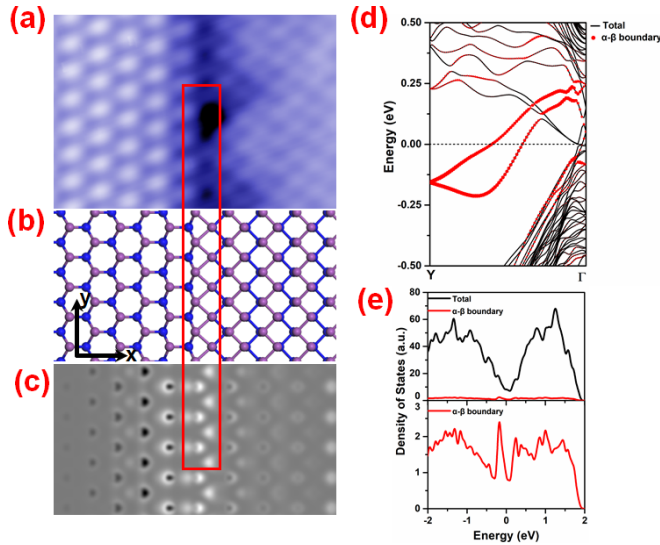


FIG. 5. Electronic properties of the α - β homojunction. (a) Experimental STM image of a sharp interface between α and β -bismuthene. (b) Theoretically optimized in-plane interface comprising (left) β - and (right) α -bismuthene. The red rectangle indicates the boundary of the α - β homojunction. (c) Simulated STM image of the interface with constant height. Because the atoms along the phase boundary are higher than neighboring domains, the simulated STM image shows brighter spots along the edge. Black spots on the left side suggest the higher Bi atoms. Side view of the homojunction is shown in Fig. S7(a) in the Supplemental Material [60]. (d) The band structure of α - β homojunction along the y axis in (b) with SOC. The red dots show the occupancy of the α - β boundary atoms. (e) DOS of α - β homojunction with SOC. Top: DOS of the total and α - β boundary. Bottom: Enlarged projected DOS of the α - β boundary. The Fermi energy is shifted to 0 eV.

calculated band structure of the α - β homojunction along the direction of the boundary is shown in Fig. 5(d); there are two prominent dispersive bands crossing the Fermi level originating from the boundary. Furthermore, our calculation shows a nonzero DOS near the Fermi energy, which is characteristic of a metallic feature [bottom panel of Fig. 5(e)]. To further confirm the boundary effect, we investigated the edge state of an ~ 8 -nm wide nanoribbon composed of α - β homojunction (Fig. S7(b) in the Supplemental Material [60]). The band structures and DOS of the edges of α - and β phases show the similar electrical occupation with the α - β homojunction (Figs. S7(c) and S7(d) in the Supplemental Material [60]). Furthermore, the β -bismuthene is a nontrivial TI that demonstrates an edge state along the ordered zigzag boundary. The α -bismuthene with a buckling height larger than 0.1 Å is a

trivial semiconductor. In the current case, the Bi atoms in the top layer of α -bismuthene are heavily buckled with a height of 0.65 Å, thus showing no topological properties[11]. Consequently, the edge state on the zigzag edge of the β -bismuthene can be preserved. It can be concluded that the topological state occurs on the boundary of the α - β homojunction.

Clearly, experimental spectroscopy measurements can provide more precise characterization of the properties of edge states. Ultimately, if such homojunction prepared on insulating substrates terminated with one monolayer copper oxide can match what we found in this work by phase transition, these 1D homojunctions can be exploited for devices with topologically protected edge states [66,67].

IV. SUMMARY AND CONCLUSIONS

In summary, we studied the phase transition from single-layer α -bismuthene to β -bismuthene on $\text{Cu}_3\text{O}_2/\text{Cu}(111)$ by means of thermal annealing. Theoretical calculations along with high-resolution STM images demonstrate a bond-breaking pathway during the phase transition. Phase transition induces the formation of an atomically sharp interface between α - and β -bismuthene that allows us to study their electronic properties. On the $\text{Cu}_3\text{O}_2/\text{Cu}(111)$ substrate, the α phase with a buckling height larger than 0.1 Å can be stabilized, while thermal annealing induced phase transition generates an atomically sharp homojunction comprising zigzag Bi atoms. DFT calculations reveal the edge states along the homojunction. Our result provides a way to realize one-dimensional edge state at the phase boundary of the strong spin-orbit-coupling systems.

ACKNOWLEDGMENTS

This work is financially supported by the Natural Science Foundation of Jiangsu Province (Grant No. BK20181297), the National Natural Science Foundation of China (Grants No. 61574123, No. 11974307, No. 11874427, and No. 11790313), and the Fundamental Research Funds for Central Universities (Grants No. 30919011257 and No. 2019FZA3004), Zhejiang Provincial Natural Science Foundation (Grant No. D19A040001), and the 2DMOST, Shenzhen Univ. (Grant No. 2018028) and China Scholarship Council (Grant No.202006840040). The DFT computations in this paper were run on the Tianhe-II of the National Supercomputer Center in Guangzhou and the π 2.0 cluster supported by the Center for High Performance Computing at Shanghai Jiao Tong University. We acknowledge Y. Gao and Dr. J. Zhang (NUS) for providing the chemicals, and Dr. J. Gou (NUS) for helpful discussion.

[1] P. Hofmann, *Prog. Surf. Sci.* **81**, 191 (2006).
 [2] T. Hirahara, T. Nagao, I. Matsuda, G. Bihlmayer, E. V. Chulkov, Y. M. Koroteev, P. M. Echenique, M. Saito, and S. Hasegawa, *Phys. Rev. Lett.* **97**, 146803 (2006).

[3] Y. M. Koroteev, G. Bihlmayer, J. E. Gayone, E. V. Chulkov, S. Blügel, P. M. Echenique, and P. Hofmann, *Phys. Rev. Lett.* **93**, 046403 (2004).
 [4] S. Murakami, *Phys. Rev. Lett.* **97**, 236805 (2006).

- [5] Y. L. Chen, J. G. Analytis, J. H. Chu, Z. K. Liu, S. K. Mo, X. L. Qi, H. J. Zhang, D. H. Lu, X. Dai, Z. Fang, S. C. Zhang, I. R. Fisher, Z. Hussain, and Z. X. Shen, *Science* **325**, 178 (2009).
- [6] M. Wada, S. Murakami, F. Freimuth, and G. Bihlmayer, *Phys. Rev. B* **83**, 121310(R) (2011).
- [7] Z. Liu, C.-X. Liu, Y.-S. Wu, W.-H. Duan, F. Liu, and J. Wu, *Phys. Rev. Lett.* **107**, 136805 (2011).
- [8] Y. M. Koroteev, G. Bihlmayer, E. V. Chulkov, and S. Blügel, *Phys. Rev. B* **77**, 045428 (2008).
- [9] H. W. Yeom, K. H. Jin, and S. H. Jhi, *Phys. Rev. B* **93**, 075435 (2016).
- [10] S.-S. Li, W.-X. Ji, P. Li, S.-J. Hu, L. Cai, C.-W. Zhang, and S.-S. Yan, *ACS Appl. Mater. Interfaces* **9**, 21515 (2017).
- [11] Y. Lu, W. Xu, M. Zeng, G. Yao, L. Shen, M. Yang *et al.*, *Nano Lett.* **15**, 80 (2015).
- [12] F. Reis, G. Li, L. Dudy, M. Bauernfeind, S. Glass, W. Hanke, R. Thomale, J. Schäfer, and R. Claessen, *Science* **357**, 287 (2017).
- [13] M. Zhou, W. Ming, Z. Liu, Z. Wang, P. Li, and F. Liu, *Proc. Natl. Acad. Sci. USA* **111**, 14378 (2014).
- [14] M. Pumera and Z. Sofer, *Adv. Mater.* **29**, 1605299 (2017).
- [15] P. J. Kowalczyk, O. Mahapatra, D. N. McCarthy, W. Kozłowski, Z. Klusek, and S. A. Brown, *Surf. Sci.* **605**, 659 (2011).
- [16] J. Gou, L. Kong, X. He, Y. L. Huang, J. Sun, S. Meng, K. Wu, L. Chen, and A. T. S. Wee, *Sci. Adv.* **6**, eaba2773 (2020).
- [17] T. R. J. Bollmann, R. van Gastel, H. J. W. Zandvliet, and B. Poelsema, *Phys. Rev. Lett.* **107**, 176102 (2011).
- [18] K. Gärtler and K. Jacobi, *Surf. Sci.* **152–153**, 272 (1985).
- [19] Y. Girard, C. Chacon, G. de Abreu, J. Lagoute, V. Repain, and S. Rousset, *Surf. Sci.* **617**, 118 (2013).
- [20] D. Kaminski, P. Poodt, E. Aret, N. Radenovic, and E. Vlieg, *Surf. Sci.* **575**, 233 (2005).
- [21] C. Kato, Y. Aoki, and H. Hirayama, *Phys. Rev. B* **82**, 165407 (2010).
- [22] K. H. L. Zhang, I. M. McLeod, Y. H. Lu, V. R. Dhanak, A. Matilainen, M. Lahti, K. Pussi, R. G. Egdel, X. S. Wang, A. T. S. Wee, and W. Chen, *Phys. Rev. B* **83**, 235418 (2011).
- [23] N. Kawakami, C. L. Lin, K. Kawahara, M. Kawai, R. Arafune, and N. Takagi, *Phys. Rev. B* **96**, 205402 (2017).
- [24] B. He, G. Tian, J. Gou, B. Liu, K. Shen, Q. Tian, Z. Yu, F. Song, H. Xie, Y. Gao, Y. Lu, K. Wu, L. Chen, and H. Huang, *Surf. Sci.* **679**, 147 (2019).
- [25] J. H. Jeon, K. H. Chung, H. Kim, and S.-J. Kahng, *Surf. Sci.* **603**, 145 (2009).
- [26] C. H. Chen, K. D. Kepler, A. A. Gewirth, B. M. Ocko, and J. Wang, *J. Phys. Chem.* **97**, 7290 (1993).
- [27] C. A. Jeffrey, D. A. Harrington, and S. Morin, *Surf. Sci.* **512**, L367 (2002).
- [28] J. T. Sadowski, T. Nagao, S. Yaginuma, Y. Fujikawa, T. Sakurai, A. Oreshkin, M. Saito, and T. Ohno, *J. Appl. Phys.* **99**, 014904 (2006).
- [29] T. Nagao, J. T. Sadowski, M. Saito, S. Yaginuma, Y. Fujikawa, T. Kogure, T. Ohno, Y. Hasegawa, S. Hasegawa, and T. Sakurai, *Phys. Rev. Lett.* **93**, 105501 (2004).
- [30] S. Yaginuma, K. Nagaoka, T. Nagao, G. Bihlmayer, Y. M. Koroteev, E. V. Chulkov, and T. Nakayama, *J. Phys. Soc. Jpn.* **77**, 014701 (2007).
- [31] R. Shioda, A. Kawazu, A. A. Baski, C. F. Quate, and J. Nogami, *Phys. Rev. B* **48**, 4895 (1993).
- [32] A. Goriachko, P. V. Melnik, A. Shchyrba, S. P. Kulyk, and M. G. Nakhodkin, *Surf. Sci.* **605**, 1771 (2011).
- [33] C.-H. Hsu, H.-R. Chang, F.-C. Chuang, Y.-T. Liu, Z.-Q. Huang, H. Lin, V. Ozolinš, and A. Bansil, *Surf. Sci.* **626**, 68 (2014).
- [34] Y. Ohtsubo, S. Hatta, M. Iwata, K. Yaji, H. Okuyama, and T. Aruga, *J. Phys.: Condens. Matter* **21**, 405001 (2009).
- [35] T. Hirahara, G. Bihlmayer, Y. Sakamoto, M. Yamada, H. Miyazaki, S.-i. Kimura, S. Blügel, and S. Hasegawa, *Phys. Rev. Lett.* **107**, 166801 (2011).
- [36] F. Yang, L. Miao, Z. F. Wang, M. Y. Yao, F. Zhu, Y. R. Song, M. X. Wang, J. P. Xu, A. V. Fedorov, Z. Sun *et al.*, *Phys. Rev. Lett.* **109**, 016801 (2012).
- [37] M. Chen, J. P. Peng, H. M. Zhang, L. L. Wang, K. He, X. C. Ma, and Q. K. Xue, *Appl. Phys. Lett.* **101**, 081603 (2012).
- [38] S. H. Kim, K. H. Jin, J. Park, J. S. Kim, S. H. Jhi, T. H. Kim, and H. W. Yeom, *Phys. Rev. B* **89**, 155436 (2014).
- [39] K. Yamada, S. Souma, K. Yamauchi, N. Shimamura, K. Sugawara, C. X. Trang, T. Oguchi, K. Ueno, T. Takahashi, and T. Sato, *Nano Lett.* **18**, 3235 (2018).
- [40] L. Peng, J.-J. Xian, P. Tang, A. Rubio, S.-C. Zhang, W. Zhang, and Y.-S. Fu, *Phys. Rev. B* **98**, 245108 (2018).
- [41] L. Peng, J. Qiao, J.-J. Xian, Y. Pan, W. Ji, W. Zhang, and Y.-S. Fu, *ACS Nano* **13**, 1885 (2019).
- [42] A. Fang, C. Adamo, S. Jia, R. J. Cava, S.-C. Wu, C. Felser, and A. Kapitulnik, *Sci. Adv.* **4**, eaaq0330 (2018).
- [43] H. H. Sun, M. X. Wang, F. F. Zhu, G. Y. Wang, H. Y. Ma, Z. A. Xu, Q. Liao, Y. H. Lu, C. L. Gao, Y. Y. Li, C. H. Liu, D. Qian, D. D. Guan, and J. F. Jia, *Nano Lett.* **17**, 3035 (2017).
- [44] D. Zhou, H. Li, N. Si, H. Li, H. Fuchs, and T. Niu, *Adv. Funct. Mater.* **31**, 2006997 (2021).
- [45] D. Tristant, A. Cupo, and V. Meunier, *2D Mater.* **5**, 035044 (2018).
- [46] C. Hogan, K. Holtgrewe, F. Ronci, S. Colonna, S. Sanna, P. Moras, P. M. Sheverdyaeva, S. Mahatha, M. Papagno, Z. S. Aliev, M. Babanly, E. V. Chulkov, C. Carbone, and R. Flammini, *ACS Nano* **13**, 10481 (2019).
- [47] Z.-Q. Shi, H. Li, Q.-Q. Yuan, C.-L. Xue, Y.-J. Xu, Y.-Y. Lv, Z.-Y. Jia, Y. Chen, W. Zhu, and S.-C. Li, *ACS Nano* **14**, 16755 (2020).
- [48] Z.-Q. Shi, H. Li, Q.-Q. Yuan, Y.-H. Song, Y.-Y. Lv, W. Shi, Z.-Y. Jia, L. Gao, Y.-B. Chen, W. Zhu, and S.-C. Li, *Adv. Mater.* **31**, 1806130 (2019).
- [49] F. Schindler, Z. Wang, M. G. Vergniory, A. M. Cook, A. Murani, S. Sengupta, A. Y. Kasumov, R. Deblock, S. Jeon, I. Drozdov, H. Bouchiat, S. Guéron, A. Yazdani, B. A. Bernevig, and T. Neupert, *Nat. Phys.* **14**, 918 (2018).
- [50] J. Moore, *Nat. Phys.* **5**, 378 (2009).
- [51] D. Zhou, N. Si, B. Jiang, X. Song, H. Huang, Q. Ji, and T. Niu, *Adv. Mater. Interfaces* **6**, 1901050 (2019).
- [52] G. Kresse and J. Hafner, *Phys. Rev. B* **47**, 558 (1993).
- [53] J. P. Perdew, K. Burke, and M. Ernzerhof, *Phys. Rev. Lett.* **77**, 3865 (1996).
- [54] P. E. Blöchl, *Phys. Rev. B* **50**, 17953 (1994).
- [55] J. Klimeš, D. R. Bowler, and A. Michaelides, *J. Phys.: Condens. Matter* **22**, 022201 (2009).
- [56] G.-R. Qian, X. Dong, X.-F. Zhou, Y. Tian, A. R. Oganov, and H.-T. Wang, *Comput. Phys. Commun.* **184**, 2111 (2013).
- [57] A. R. Oganov, A. O. Lyakhov, and M. Valle, *Acc. Chem. Res.* **44**, 227 (2011).

- [58] A. R. Oganov and C. W. Glass, *J. Chem. Phys.* **124**, 244704 (2006).
- [59] T. Niu, Q. Meng, D. Zhou, N. Si, S. Zhai, X. Hao, M. Zhou, and H. Fuchs, *Adv. Mater.* **32**, 1906873 (2020).
- [60] See Supplemental Material at <http://link.aps.org/supplemental/10.1103/PhysRevMaterials.5.064002> for STM images of copper oxide/Cu(111) surface, atomic structure of β - and α -bismuthene, temperature-dependent phase transition, bias-dependent STM images at the interface of α - and β -bismuthene, the atomic model and band structures of α - and β -bismuthene, the atomic model and band structures of α - and β -bismuthene with experimental lattice parameter, and electrical properties of the α - β homojunction.
- [61] A. S. Rodin, A. Carvalho, and A. H. Castro Neto, *Phys. Rev. Lett.* **112**, 176801 (2014).
- [62] Y. H. Mao, L. F. Zhang, H. L. Wang, H. Shan, X. F. Zhai, Z. P. Hu, A. D. Zhao, and B. Wang, *Front. Phys.* **13**, 138106 (2018).
- [63] Z. Zhu and D. Tománek, *Phys. Rev. Lett.* **112**, 176802 (2014).
- [64] Y. R. Luo, *Comprehensive Handbook of Chemical Bond Energies* (CRC Press, Boca Raton, 2007).
- [65] D. Zhou, Q. Meng, N. Si, X. Zhou, S. Zhai, Q. Tang, Q. Ji, M. Zhou, T. Niu, and H. Fuchs, *ACS Nano* **14**, 2385 (2020).
- [66] I. K. Drozdov, A. Alexandradinata, S. Jeon, S. Nadj-Perge, H. Ji, R. J. Cava, B. A. Bernevig, and A. Yazdani, *Nat. Phys.* **10**, 664 (2014).
- [67] Z. Pedramrazi, C. Herbig, A. Pulkin, S. Tang, M. Phillips, D. Wong, H. Ryu, M. Pizzochero, Y. Chen, F. Wang, E. J. Mele, Z.-X. Shen, S.-K. Mo, O. V. Yazyev, and M. F. Crommie, *Nano Lett.* **19**, 5634 (2019).